J. Fluid Mech. (1980), *vol.* 98, *part* 3, *pp.* 635–645
Printed in Great Britain

The effects of shear and vorticity on deformation of a drop

By F. S. HAKIMI† AND W. R. SCHOWALTER
Department of Chemical Engineering, Princeton University,
New Jersey 08540

(Received 22 August 1978 and in revised form 28 December 1979)

A fluid drop immersed in a second incompressible fluid is deformed by a motion which, far from the drop, varies linearly with distance. Deformation of the drop is then determined by both the rate of deformation and the vorticity of the continuous fluid phase far from the drop. Experiments are described in which the vorticity and rate of deformation were independently varied by means of an eccentric-disk rheometer field. It is shown that predictions from a small-parameter expansion to first order in $\epsilon = \mu_0 Gb/\sigma$ are in good agreement with experiment to values of ϵ as large as 0·4, where μ_0 is viscosity of the continuous phase, G a measure of the flow strength, b the drop radius, and σ the interfacial tension.

Of the several terms which arise in the $O(\epsilon)$ expansion, only that one which contains a Jaumann derivative of the deformation parameter provides an important contribution beyond Taylor's original analysis of the problem. This fact greatly simplifies the computation of drop shape.

1. Introduction

There are several motivations for studying the response of a fluid drop to the motion of a second fluid phase surrounding the drop. The multiphase nature of the problem is a special challenge to fluid mechanists because of the effect of flow on the location of the boundary separating continuous and discontinuous phases. The problem also represents the basic unit governing the behaviour of emulsions in technologically important flows. Finally, it has become apparent that many qualitative features of rheologically complex fluids, examples being polymer solutions and polymer melts, are shared with the bulk properties of two-phase mixtures. In particular, dilute two-phase systems (i.e. systems for which interactions between segments of the discontinuous phase are not important) hold a special attraction as models of rheologically complex fluids, because macroscopic bulk behaviour of the mixture can often be computed in terms of fundamental properties of each individual phase. Thus one has a model with identifiable physical parameters and a means to compute bulk constitutive behaviour in terms of these parameters.

Relevant to the present work are the studies of Schowalter, Chaffey & Brenner (1968) of the effect of drop deformation on the rheology of a dilute emulsion of two Newtonian fluids, the extension of that work to more general situations by Frankel & Acrivos (1970), and analyses by Cox (1969) and by Barthès-Biesel & Acrivos (1973).

† Present address: Amoco Minerals Company, Chicago, Illinois 60601.

0022-1120/80/4519-1530 $02.00

Cox and Frankel & Acrivos showed how to predict the shape of a slightly deformed Newtonian drop when it is surrounded by a second Newtonian phase which, at large distances from the drop, possesses a velocity field varying linearly with distance. These results were extended to higher order in the deformation by Barthès-Biesel & Acrivos. A unification of these analyses has been provided by Rallison (1980).

One of the interesting features of the foregoing analyses is a prediction that the drop shape is affected differently by the symmetric and the antisymmetric portions of the far-field velocity gradient; i.e. by both the rate of deformation and the vorticity. This result has important rheological implications, because the constitutive equation representing the behaviour of the multiphase bulk system will clearly be sensitive to the shape of the discontinuous phase (Schowalter 1979). The importance of the different effects of rate of deformation and vorticity does not seem to have been fully appreciated, probably because in all of the examples for which drop shape has been calculated, and in most of the viscometers in which rheological properties are determined, there is a one-to-one relation between rate of deformation and vorticity; as soon as the rate of deformation is determined, the vorticity is also fixed. Examples of the most common prototype flows for which one is likely to see calculations are laminar shear flows (such as Couette flow), where the non-zero components of the rate of deformation and the vorticity are numerically equal, and uniaxial extension or compression, for which the vorticity is zero.

Because of the desire to explore the different effects of vorticity and rate of deformation on drop shape, and because of the known importance of the relative amounts of vorticity and rate of deformation on drop and cluster breakup, it was decided to study drop shape in a flow different from those used heretofore. In the flow field of an eccentric-disk rheometer (also called an orthogonal rheometer) one is at liberty independently to alter the rate of deformation and the vorticity within the limits of weak flows; i.e. a norm of the ratio of rate of deformation to vorticity can be varied between zero and unity. Consequently, this flow geometry is convenient for our purposes, and we have studied the shape of single drops in the flow field generated by an orthogonal rheometer. Excellent agreement was obtained between predictions for drop shape and experimental results.

In § 2 we review the flow which obtains in an orthogonal rheometer flow field and provide an expression for drop shape. Section 3 contains a description of experimental apparatus and procedure for studying the shape of a single drop in an orthogonal rheometer. Experimental results are presented in § 4.

2. Orthogonal rheometer flow field

Kinematics

The most comprehensive analysis of the eccentric-disk rheometer is that of Abbott & Walters (1970). The flow field is shown schematically in figure 1. Two circular parallel disks are each rotated at angular speed Ω. Fluid is contained in the gap, of height h, separating the disks. The fluid is subjected to a combination of shear and rotation which is governed by the rotational speed Ω and the offset a of the centre of rotation of one disk relative to the other. Abbott & Walters have shown that if inertial effects are negligible; i.e. $[\rho\Omega/2\mu]^{\frac{1}{2}}h \ll 1$, where ρ is the fluid density and μ the viscosity, then at any value of z the flow is a solid-body rotation about the point at z on a line

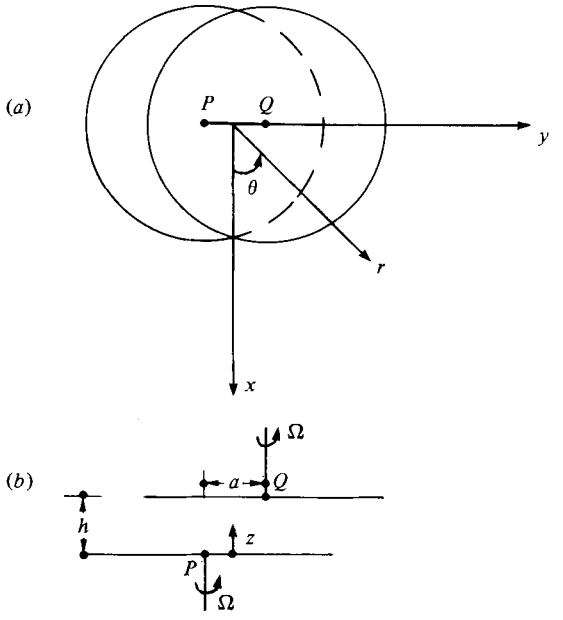

FIGURE 1. Schematic diagram of the eccentric-disk rheometer, (*a*) top view, (*b*) front view.

joining the centres of rotation of the two disks. Thus, with respect to the axes of figure 1,

$$v_x = -\Omega y + \Omega\psi z, \quad v_y = \Omega x, \quad v_z = 0, \tag{2.1}$$

where the eccentricity is given by $\psi = a/h$. Deformation rate and vorticity, respectively, are

$$e_{ij} = \tfrac{1}{2}(\partial v_i/\partial x_j + \partial v_j/\partial x_i),$$

$$[\mathbf{e}] = \frac{\Omega\psi}{2}\begin{bmatrix} 0 & 0 & 1 \\ 0 & 0 & 0 \\ 1 & 0 & 0 \end{bmatrix}, \tag{2.2}$$

$$\omega_{ij} = \tfrac{1}{2}(\partial v_i/\partial x_j - \partial v_j/\partial x_i),$$

$$[\boldsymbol{\omega}] = \Omega\begin{bmatrix} 0 & -1 & \frac{1}{2}\psi \\ 1 & 0 & 0 \\ -\frac{1}{2}\psi & 0 & 0 \end{bmatrix}. \tag{2.3}$$

Components of the vorticity vector are ω_k, where ω_k is defined by $\omega_{ij} = -\frac{1}{2}\epsilon_{ijk}\omega_k$. Thus

$$(\omega_k) = (0,\ \Omega\psi,\ 2\Omega). \tag{2.4}$$

It is immediately apparent from (2.2) and (2.3) that one can independently alter the magnitude of $\mathbf{e}$ and $\boldsymbol{\omega}$ through suitable combinations of Ω and ψ. This is to be contrasted, for example, with the laminar shear flow $v_1 = \kappa x_3$, for which $e_{ij} = \pm\omega_{ij}$; or with extensional flows (pure shear), for which $\omega_{ij} = 0$.

Drop shape

We shall be concerned solely with the weak flow case discussed by Rallison (1980). Here $k > 1$, $\lambda = o(k)$, where $k = \sigma/\mu_0 Gb$, $\epsilon = k^{-1}$, and $\lambda = \mu^*/\mu_0$. Interfacial tension is given by σ, b is the radius of the undeformed spherical drop, μ_0 and μ^* are viscosities

of the continuous and discontinuous phases, respectively, and G is a measure (for example, the second invariant) of the rate-of-deformation tensor. Drop shape is given by

$$r = 1 + \epsilon f(x_i/r) + O(\epsilon^2), \tag{2.5}$$

$$f = F_{ij}\left(\frac{\partial^2 r^{-1}}{\partial x_i\,\partial x_j}\right)_{r=1} + \epsilon\left\{-\tfrac{6}{5}F_{ij}F_{ij} + H_{ijkl}\left[\frac{\partial^4 r^{-1}}{\partial x_i\,\partial x_j\,\partial x_k\,\partial x_l}\right]_{r=1}\right\} \tag{2.6}$$

and the coefficients F_{ij} and H_{ijkl} are governed by equations (5) and (6) of Rallison (1980), which we reproduce here:

$$\epsilon\frac{\mathscr{D}F_{ij}}{\mathscr{D}t} = a_0 e_{ij} + a_1 F_{ij} + \epsilon a_2 Sd(e_{il}F_{lj}) + \epsilon a_3 Sd(F_{il}F_{lj}) + O(\epsilon^2), \tag{2.7}$$†

$$\epsilon\frac{\mathscr{D}H_{ij}}{\mathscr{D}t} = b_0 H_{ij} + b_1 Sd_4(e_{il}F_{lj}) + b_2 Sd_4(F_{il}F_{lj}) + O(\epsilon). \tag{2.8}$$

Coefficients in (2.7) are

$$a_0 = \frac{5}{3(2\lambda+3)}, \quad a_2 = \frac{10(4\lambda-9)}{7(2\lambda+3)^2},$$

$$a_1 = -\frac{40(\lambda+1)}{(2\lambda+3)(19\lambda+16)}, \quad a_3 = \frac{288(137\lambda^3+624\lambda^2+741\lambda+248)}{7(2\lambda+3)^2(19\lambda+16)^2},$$

$$b_0 = \frac{-360(\lambda+1)}{(17\lambda+16)(10\lambda+11)}, \quad b_1 = \frac{1}{7(2\lambda+3)},$$

$$b_2 = \frac{16(-14\lambda^3+207\lambda^2+431\lambda+192)}{21(2\lambda+3)(19\lambda+16)(17\lambda+16)(10\lambda+11)},$$

and variables with units of time have been made dimensionless with $G = \Omega\psi$. For any tensor with components a_{ij} or a_{ijkl},

$$Sd(a_{ij}) = \tfrac{1}{2}(a_{ij}+a_{ji}) - \tfrac{1}{3}\delta_{ij}a_{ll}.$$

$$\begin{aligned} Sd_4(a_{ijkl}) = {} & \tfrac{1}{8}[\text{the sum of 24 permutations of } a_{ijkl}] - \tfrac{1}{28}\{\text{the sum of 6 permutations of } [\delta_{ij}(\text{the sum of 12 permutations of } a_{klmm})]\} \\ & + \tfrac{1}{35}(\delta_{ij}\delta_{kl}+\delta_{ik}\delta_{jl}+\delta_{il}\delta_{jk})(a_{mmnn}+a_{mnmn}+a_{mnnm}). \end{aligned}$$

We wish to compare predictions of drop shape, at steady state, with the results of experiments described below. In general the solution of coupled nonlinear equations (2.7) and (2.8) is required, and it is natural to consider approximate solutions. The simplest is to retain only

$$a_0 e_{ij} + a_1 F_{ij} = 0. \tag{2.9}$$

This, of course, is the expression used by Taylor (1934) and is known to be followed in the limit of small deformations.

† The Jaumann time derivative often occurs in constitutive expressions for rheologically complex materials. It is a time derivative relative to axes rotating with angular velocity $\frac{1}{2}\boldsymbol{\omega}$ in a laboratory-fixed frame of reference

$$\frac{\mathscr{D}F_{ij}}{\mathscr{D}t} = \frac{\partial F_{ij}}{\partial t} + \tfrac{1}{2}\omega_k(\epsilon_{lki}F_{lj} + \epsilon_{lkj}F_{li}).$$

The next step one might consider is to include the Jaumann derivative in (2.7) but to retain a linear, uncoupled equation. Then

$$\epsilon \frac{\mathscr{D}F_{ij}}{\mathscr{D}t} \cong a_0 e_{ij} + a_1 F_{ij}. \tag{2.10}$$

A solution can readily be obtained, and one finds

$$\begin{aligned}
F_{11} &= M[4N^2 + (W/G)^2], \\
F_{22} &= 12M(\Omega/G)^2, \\
F_{33} &= -M[4N^2 + 4(W/G)^2 - 3], \\
F_{12} &= F_{21} = 6MN\Omega/G, \\
F_{13} &= F_{31} = MN[4N^2 + 4(W/G)^2 - 3], \\
F_{23} &= F_{32} = 2M(\Omega/G)\,[2N^2 + 2(W/G)^2 - 3],
\end{aligned} \tag{2.11}$$

where

$$G = \Omega\psi, \quad W = \Omega(4+\psi^2)^{\frac{1}{2}},$$

$$M = \frac{5k}{6(2\lambda+3)\,[4N^2 + (W/G)^2][N^2 + (W/G)^2]},$$

$$N = \frac{40k(\lambda+1)}{(2\lambda+3)\,(19\lambda+16)},$$

and we have set $\epsilon = k^{-1}$.

3. Experiments

Flow apparatus

The objective of the experiments was to measure small deformations of a drop suspended in a continuous phase, which at large distances from the drop, is undergoing the motion described by (2.1). The flow was generated with a modified Model R16 Weissenberg Rheogoniometer. A diagram of the flow system is shown in figure 2. The lower plate, which was fastened to the rotating member of the rheogoniometer, had an inner diameter of 11·5 cm and a lip 1·5 cm high. Fluid was contained between this lower plate and an upper plate, which was 0·6 cm thick and 10·2 cm in diameter. Both plates were Plexiglas. The upper plate was fastened to a cylindrical Plexiglas support which was 4·5 cm high and had an inner diameter of 8·7 cm. The cylinder was in turn secured to a ring-shaped aluminium support mounted on top of an air bearing. The housing for the air bearing was connected to the main column of the rheogoniometer through a specially constructed track mechanism. The track allowed movement of the air-bearing assembly in the horizontal (y) direction, and the rheogoniometer post permitted movement of the upper plate in the vertical (z) direction. The air bearing insured rotation of the upper plate at very nearly the same rotational speed as that of the bottom plate. The bearing was built to our specifications and is described elsewhere (Hakimi 1976). Gap distance and eccentricity were read to $\pm$ 0·0002 cm with micrometer gauges.

Fluids

Following the choice of Torza, Cox & Mason (1972), we used D–B castor oil as the continuous phase because of the close correspondence between refractive indices of Plexiglass (1·474) and the castor oil (1·4774). Viscosity of the castor oil was 7·1925 P

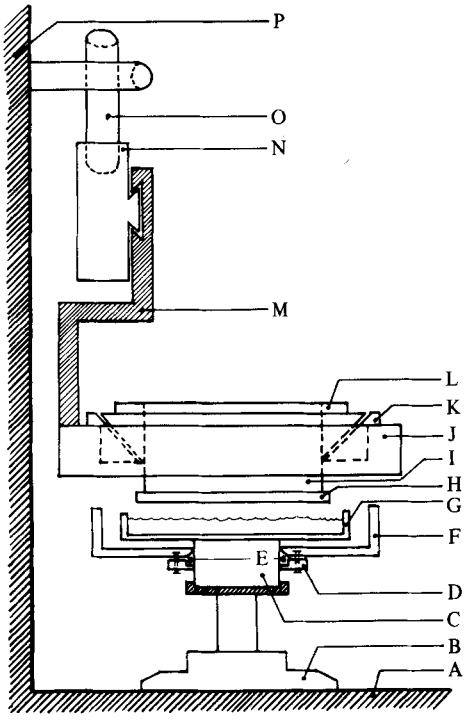

FIGURE 2. Flow apparatus. A, base of rheogoniometer; B, lower platen adapter; C, cylindrical connector; D, aluminium retainer; E, rubber O-ring; F, box container; G, lower plate of flow cell; H, upper plate of flow cell; I, cylindrical support; J, rigid support; K, air bearing; L, aluminium ring support; M, vertical block support; N, vertical support with key; O, aluminium rods; P, main column of Weissenberg rheogoniometer.

at 22 °C. Drops were formed from a mixture of two different Dow Corning silicone fluids (series 200). The mixture had a nominal refractive index of 1·40 and a viscosity at 22 °C of 0·652 P. Interfacial tension between the fluids was taken to be 4·1 dyne cm^{-1}, the value reported by the supplier of the silicone fluid and the value used by others (Torza *et al.* 1972).

Flow visualization and recording

Drop shapes were observed with a camera–microscope system which was mounted either in front of the test chamber or above it. Thus projections of drops onto the yz and xy planes were obtained. An adequate working distance and field of view were obtained by combination of a Bausch & Lomb 10× focusable eyepiece and a 1·5× Leitz Wetzler objective in a Mono lux body tube. Drops were illuminated with a focusable illuminator (American Optical Model 653A). Light from the illuminator was passed through two heat-absorbing filters to minimize temperature changes in the fluids. Illumination and observation were facilitated by surrounding the flow cell with the Plexiglas box container shown in figure 2. The container was 15·5 cm square, 2·5 cm high, and had walls 0·5 cm thick. It was filled with castor oil so that the refractive index along optical paths between the (flat) air/container and castor oil/silicone surfaces was nearly constant. Leakage from the bottom of the container was minimized with an O-ring seal, as shown in the figure. The microscope was attached, through an

adapter and bellows extension, to a Hasselblad 500C single-lens reflex camera. The camera was mounted on a rigid support with a vernier system that permitted controlled movement for alignment and focusing. Photographs were taken with Kodak Royal-Z film (A.S.A. = 1250) and developed by a procedure that raised the effective A.S.A. rating to 4500.

Experimental procedure

Before addition of fluid to the test section, the two plates were carefully aligned to insure that they were level and concentric. Also, the magnification of the camera–microscope system was calibrated by taking photographs of a ruled stage micrometer under conditions identical with those used for photographing the drop.

After addition of the castor oil, a drop of silicone fluid was inserted with a hypodermic syringe. Drop radius was nominally 1 mm. The upper plate was then placed at the desired offset and lowered from a known setting until it contacted the castor oil. The rheogoniometer was engaged and minor adjustment of the drop achieved by braking the upper plate until the drop was approximately midway between the plates and on a line joining their centres of rotation. Further details of the alignment and calibration procedure are available (Hakimi 1976).

Preliminary runs were conducted to insure reproducibility and to find ranges of parameters for which deformation was measurable but not extreme. Experiments for which photographs were taken from both the x and z directions covered nine eccentricities ranging from $0 \leqslant \psi \leqslant 0{\cdot}709$ and fifteen rotational speeds between 1·8 and 45 r.p.m. Gap settings were 0·680 cm for photographs taken in the z direction and 0·714 cm for those taken in the x direction. An average of three photographs from a given direction were taken for each run.

4. Results

Raw data from the experiments consist of photographs in the xy and yz planes of the drops when deformed in flow fields characterized by various values of ψ and Ω. These shapes can be compared to projected drop shapes predicted from the solution of (2.7)–(2.8), or the approximations (2.9) or (2.10). A comparison for the extreme case of $k^{-1} = \epsilon \geqslant 0{\cdot}44$ is shown in figure 3.

A more efficient presentation of the results is to compare measured and computed drop shapes by means of a deformation parameter $D = (L-B)/(L+B)$, L and B being the length and breadth, respectively, of the drop. These values for drop projections are designated D_{xy}, D_{yz}, etc. Orientation of the drop projections is designated by ϕ_{ij}. Thus ϕ_{xy} is the angle between the major axis of the xy projection of a drop and the x axis. Likewise ϕ_{yz} is the angle between the major axis of the yz projection and the y axis.

In figures 4–7 we show these quantities for selected experiments, along with the corresponding theoretical predictions based upon (2.7)–(2.8) and the approximation (2.10). One notes, in accord with theory, that drop shape and orientation depend upon both vorticity and rate of deformation of the surrounding flow field. Probably the most interesting facet of the results is the good agreement between experiments and small-deformation theory for values of the expansion parameter approaching $\epsilon = 0{\cdot}4$ and deformation parameter $D \simeq 0{\cdot}2$.

Implicit in the calculations are the shape and orientation of the deformed drop

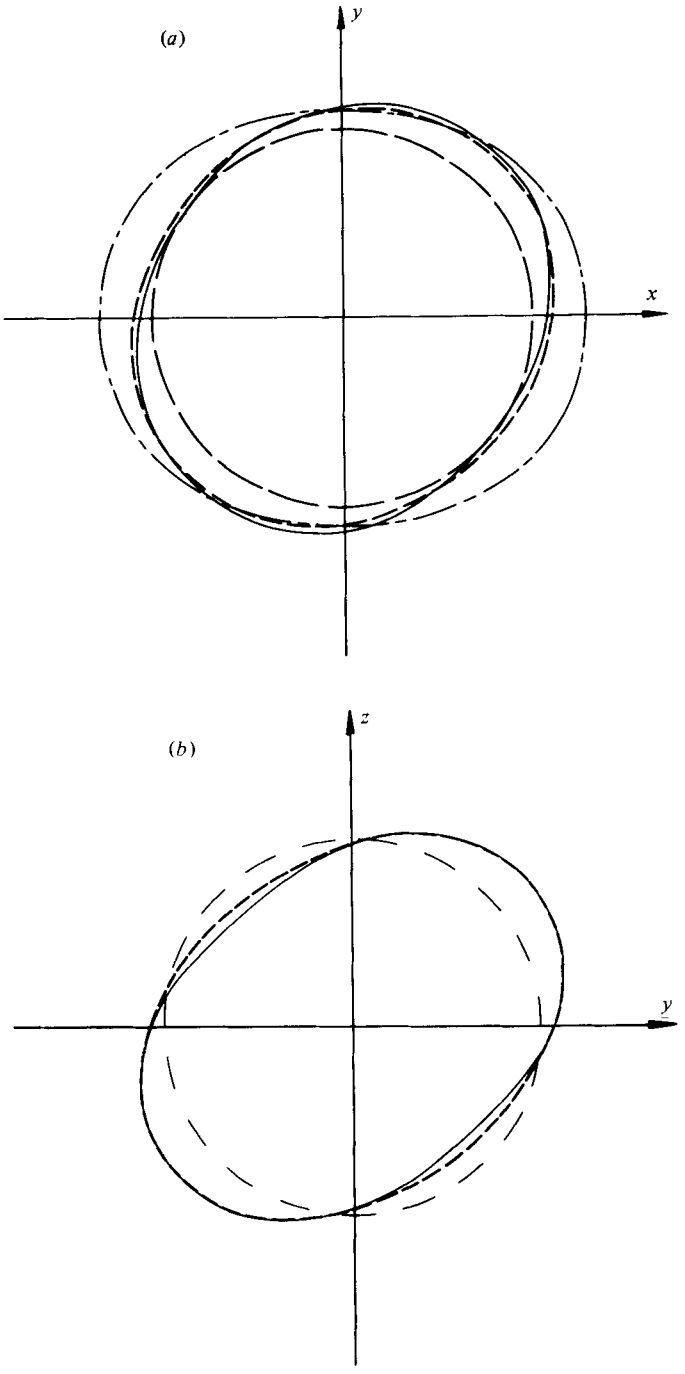

FIGURE 3. Projection of drop shape. (*a*) The xy projection for $\psi = 0{\cdot}577$, $\Omega = 4{\cdot}72\ \mathrm{s}^{-1}$, $\epsilon = k^{-1} = 0{\cdot}478$. (*b*) The yz projection for $\psi = 0{\cdot}532$, $\Omega = 4{\cdot}72\ \mathrm{s}^{-1}$, $\epsilon = k^{-1} = 0{\cdot}440$. ——, theory, equations (2.7)–(2.8); - - -, experiment; – – –, undeformed drop; – · – · –, equation (2.9).

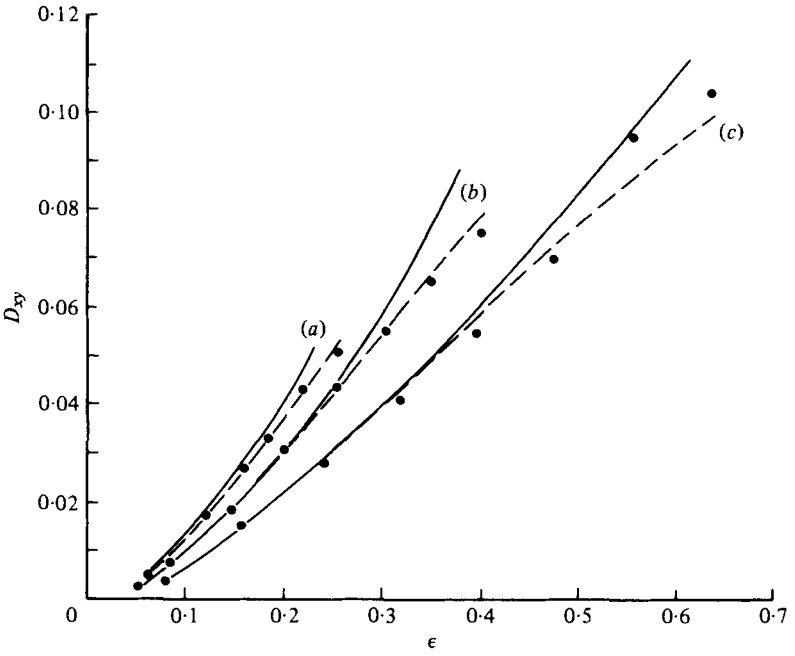

FIGURE 4. Variation of D_{xy} with expansion parameter ϵ. ——, equations (2.7)–(2.8); – – –, equation (2.10); ●, experiment. (*a*) $\Omega = 1{\cdot}88\ \mathrm{s}^{-1}$; (*b*) $\Omega = 2{\cdot}97\ \mathrm{s}^{-1}$; (*c*) $\Omega = 4{\cdot}72\ \mathrm{s}^{-1}$.

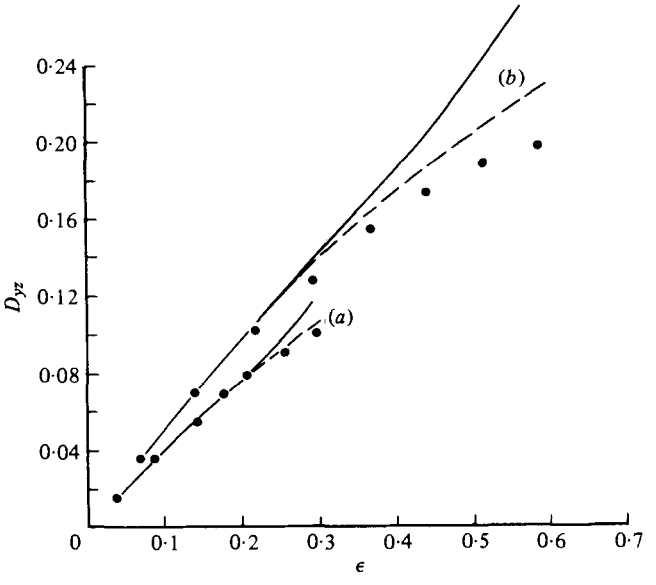

FIGURE 5. Variation of D_{yz} with expansion parameter ϵ. ——, equations (2.7)–(2.8); – – –, equation (2.10); ●, experiment. (*a*) $\Omega = 2{\cdot}36\ \mathrm{s}^{-1}$; (*b*) $\Omega = 4{\cdot}72\ \mathrm{s}^{-1}$.

itself, rather than its projections. Those results, although available, are not readily compared to experimental data and hence have not been included here.

It is of interest to note from figure 4 and 5 that equation (2.10), which differs from the Taylor solution (2.9) by inclusion of the Jaumann derivative, provides results of little difference from those of the coupled, nonlinear equations (2.7)–(2.8). In fact,

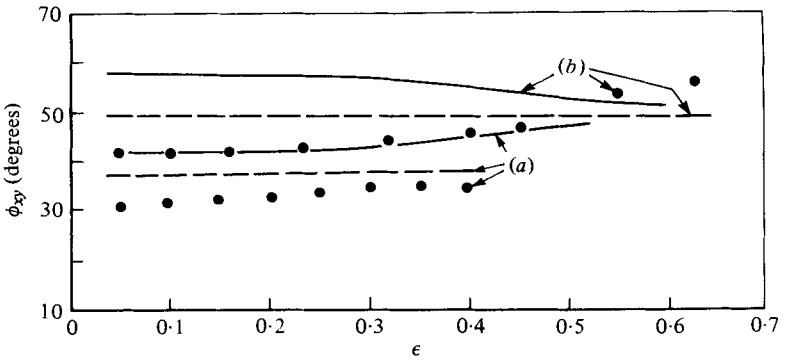

FIGURE 6. Variation of orientation angle ϕ_{xy} with expansion parameter ϵ. ——, equations (2.7)–(2.8); – – –, equation (2.10); ●, experiment. (*a*) $\Omega = 2{\cdot}9\ \mathrm{s}^{-1}$; (*b*) $\Omega = 4{\cdot}72\ \mathrm{s}^{-1}$.

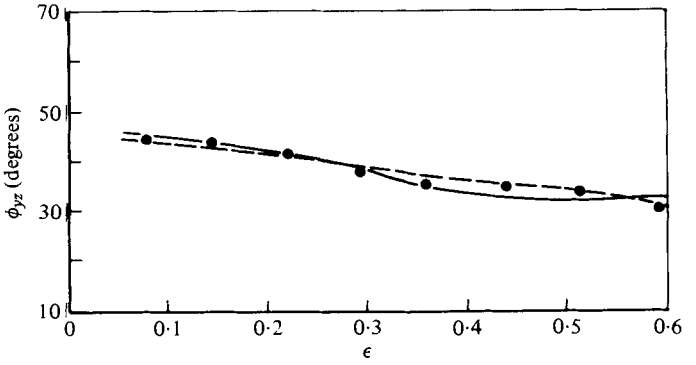

FIGURE 7. Variation of orientation angle ϕ_{yz} with expansion parameter ϵ. ——, equations (2.7)–(2.8); – – –, equation (2.10); ●, experiment. $\Omega = 4{\cdot}72\ \mathrm{s}^{-1}$.

the shapes given in figures 3(*a*) and (*b*) are nearly superposable for the two solutions. The form (2.9), however, gives poor agreement with experiment, as is evident from figure 3(*a*). Similar large differences are evident if one compares experimental projection ratios D_{xy} or D_{yz} with (2.9).

Agreement of predicted and observed drop orientation in figure 6 is less satisfactory. One can see from figure 3(*a*), however, that the measurement is subject to errors of at least $\pm 5°$. The larger deformations in the yz plane no doubt account for the better agreement in figure 7.

It is of course impossible to make a general statement concerning the validity of the approximation (2.10). One would expect, however, that the equation should be useful for weak flows for which the drop deformation is comparable to that in the experiments reported here.

5. Conclusions

The flow generated by eccentric rotating disks has been shown to be useful for studies of drop deformation because the deformation rate and the vorticity can be independently altered. Each of these affects the drop shape and orientation. Prior experimental studies of drop deformation by viscous forces have been in more conventional flow fields in which vorticity and rate of deformation are not independent.

It has been shown that the theory for drop deformation to $O(\epsilon)$ applies to values of $\epsilon \cong 0{\cdot}4$ and $D \cong 0{\cdot}2$. Furthermore, negligible accuracy is sacrificed by neglecting terms which involve products of the shape factor F_{ij} with itself or with components of the rate of deformation e_{ij}.

This research was supported in part by National Science Foundation Grant GK34427 and by the Mobil and Shell Foundations. Computations were generously supplied by M. Friedman, H. C. Lau and J. M. Rallison.

The manuscript was prepared while one of us (W. R. Schowalter) was a Sherman Fairchild Distinguished Scholar at the California Institute of Technology.

REFERENCES

Abbott, T. N. G. & Walters, K. 1970 Rheometrical flow systems. Part 2. Theory for the orthogonal rheometer, including an exact solution of the Navier–Stokes equations. *J. Fluid Mech.* **40**, 205–213.

Barthès-Biesel, D. & Acrivos, A. 1973 Deformation and burst of a liquid droplet freely suspended in a linear shear field. *J. Fluid Mech.* **61**, 1–21.

Cox, R. G. 1969 The deformation of a drop in a general time-dependent fluid flow. *J. Fluid Mech.* **37**, 601–623.

Frankel, N. A. & Acrivos, A. 1970 The constitutive equation for a dilute emulsion. *J. Fluid Mech.* **44**, 65–78.

Hakimi, F. S. 1976 The effects of shear and vorticity on the deformation of a drop. Ph.D. dissertation, Princeton University.

Rallison, J. M. 1980 Time dependent drop deformations for small deviations from sphericity. *J. Fluid Mech.* **98**, 625–633.

Schowalter, W. R. 1979 Some consequences of suspension models for non-viscometric flows. *J. Non-Newtonian Fluid Mech.* **5**, 285–296.

Schowalter, W. R., Chaffey, C. E. & Brenner, H. 1968 Rheological behaviour of a dilute emulsion. *J. Colloid Interface Sci.* **26**, 152–160.

Taylor, G. I. 1934 The formation of emulsions in definable fields of flow. *Proc. Roy. Soc.* A **146**, 501–523.

Torza, S., Cox, R. G. & Mason, S. G. 1972 Particle motions in sheared suspensions. XXVII. Transient and steady deformation and burst of liquid drops. *J. Colloid Interface Sci.* **38**, 395–411.